
# Highly Ordered Organic Ferroelectric DIPAB-Patterned Thin Films



Citation for the original published paper (version of record):
Bergenti, I., Ruani, G., Liscio, F. et al (2017). Highly Ordered Organic Ferroelectric DIPAB-Patterned Thin Films. Langmuir, 33(45): 12859-12864.
http://dx.doi.org/10.1021/acs.langmuir.7b02102

LANGMUIR

Article

Cite This: Langmuir 2017, 33, 12859-12864

pubs.acs.org/Langmuir

# Highly Ordered Organic Ferroelectric DIPAB-Patterned Thin Films

Ilaria Bergenti,*[,†] Giampiero Ruani,[†] Fabiola Liscio,[‡] Silvia Milita,[‡] Franco Dinelli,[§] Xiaofeng Xu,[∥] Ergang Wang,[∥] and Massimiliano Cavallini[†]

[†]CNR-ISMN, via Gobetti, 10140129 Bologna, Italy

[‡]CNR-IMM via Gobetti, 101 40129 Bologna, Italy

[§]CNR-INO, via Moruzzi 1, 56124 Pisa, Italy

[∥]Chalmers University of Technology, SE-412 96 Gothenburg, Sweden

**ABSTRACT:** Ferroelectric molecular compounds present great advantages for application in electronics because they combine high polarization values, comparable to those of inorganic materials, with the flexibility and low-cost properties of organic ones. However, some limitations to their applicability are related to the high crystallinity required to deploy ferroelectricity. In this article, highly ordered ferroelectric patterned thin films of diisopropylammonium bromide have been successfully fabricated by a lithographically controlled wetting technique. Confinement favors the self-organization of ferroelectric crystals, avoiding the formation of polymorphs and promoting the long-range orientation of crystallographic axes. Patterned structures present high stability, and the polarization can be switched to be arranged in stable domain pattern for application in devices.

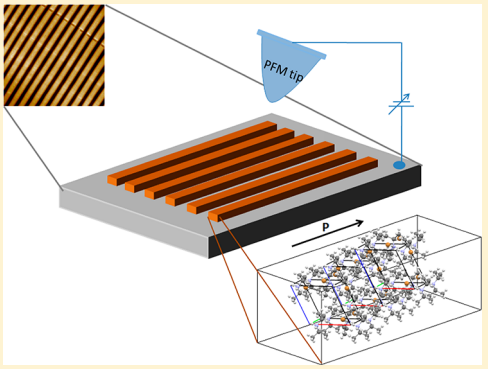


## 1. INTRODUCTION

Ferroelectrics are electroactive materials that can sustain and switch their electric polarity (ferroelectricity), sense temperature changes (pyroelectricity), interchange electric and mechanical functions (piezoelectricity), and manipulate light (through optical nonlinearities and the electro-optic effect).[1] Applications of ferroelectrics are currently dominated by inorganic materials such as PZT and BTO,[2] which present high polarization values and high stability even though they broach the topics of the presence of heavy metals and a high processing temperature. These two factors fuel the search for new substitutes with comparable electric properties. Promising alternative solutions have been found recently in hybrid organic−inorganic perovskite materials, and this field is rapidly expanding.[3] On the other hand, in the past few years significant goals have been accomplished in the field of organic ferroelectrics, which are lightweight, mechanically flexible, and environmentally friendly. Most of the current research activities focus on poly(vinylidenefluoride) (PVDF) and its related copolymers,[4] but its intrinsic low polarization ($P \approx 4.0\ \mu C/cm^2$)[5] limits its applicability in devices. An important breakthrough has been achieved by the introduction on the scientific scene of molecular crystals with ferroelectric properties (Molecular Ferroelectrics, MF):[6−8] among them, diisopropylammonium bromide (DIPAB)[9] exhibits a spontaneous polarization of 23 $\mu C\ cm^{-2}$, a Curie temperature well above RT ($T_C$ = 426 K), a remarkable piezoelectric response, low dielectric loss and well-defined ferroelectric domains, making it appealing in some practical applications to replace inorganic oxide ferroelectrics.

The whole class of MF, DIPAB included, requires stringent long-range structural order in order to deploy ferroelectric properties, and for this reason, most of the results refer to single-crystal specimens.[10,11] Few attempts to grow thin films have been made by using spin-coating techniques on surfaces and typically end up with the formation of randomly distributed microcrystals.[12] A way to extend the application of these materials in devices is to control their spontaneous tendency to crystallize in order to obtain homogeneous thin films.[13] In this work, we succeeded in mastering it by a wet lithographic method, and we obtain uniform and continuous DIPAB parallel micrometric stripes composed of coherently oriented microcrystals. In particular, we applied the lithographically controlled wetting (LCW) technique[14] exploiting the self-organizing properties of soluble materials in confinement, which was successfully used to pattern a variety of functional organic materials.[15] LCW allows us to fabricate long-range-ordered crystals with controlled shape on a scale larger than hundreds of micrometers with high uniformity in thickness and roughness, thus surpassing the overall morphological properties of microcrystals obtained by conventional wet techniques[13] without the need for any thermal annealing.[16] Our results open the way to practical applications of molecular ferroelectrics in devices filling the gap between single-crystal applications to integrated thin film technology.

**Received:** June 20, 2017
**Revised:** October 9, 2017
**Published:** October 13, 2017






DOI: 10.1021/acs.langmuir.7b02102
Langmuir 2017, 33, 12859−12864

## 2. EXPERIMENTAL SECTION

**2.1. Materials.** The DIPAB crystals were synthesized chemically by the slow evaporation of aqueous solution containing equal molar amounts of diisopropylamine and hydrobromic acid. After 3 days, needlelike transparent DIPAB crystals are obtained. The crystals were purified by recrystallization in water. Crystals were then redissolved in ultrapure water for LCW microstructures.

**2.2. Lithographically Controlled Wetting.** In LCW, a polymeric stamp is positioned in contact with the DIPAB water solution previously spread on the substrate, and the capillary action pins the solution under the stamp protrusions splitting the liquid film in separated droplets or channels. As the solution shrinks, reaching saturation, the solute precipitates onto the substrate within the menisci, giving rise to a structured thin film, in correspondence with the protrusion of the stamp. Figure 1a shows a scheme of the process.

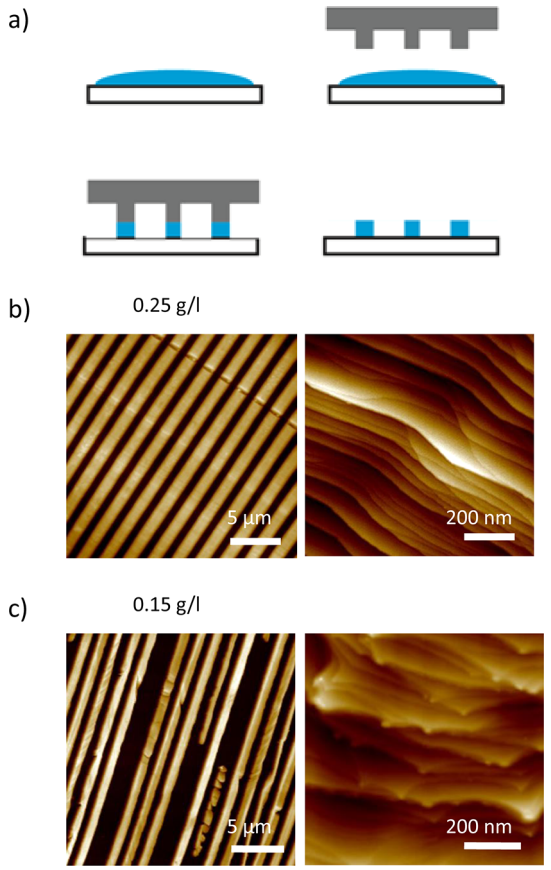


**Figure 1.** (a) Schematic representation of the LCW technique. (Left) Large-area AFM images of microstripes ($z$ scale = 0−270 nm). (Right) Detail of terraces on the surface of the stripes ($z$ scale = 0−20 nm) obtained using (b) 0.25 and (c) 0.15 g/L solution.

Because crystallization proceeds by nucleation and crystal growth, the confinement allows the control of nuclei positioning, optimizing the crystallization process. (LCW operates under quasi-equilibrium conditions.) For protocols, see Cavallini et al.[14] The geometry of the stamp defines the configuration of the final DIPAB deposit, and this technique allows us to fabricate nanostructures with size and distance controlled at multiple length scales. Here, the stamp motif consisted of parallel lines of 1 $\mu$m width spaced 1.5 $\mu$m apart. The elastomeric poly(dimethylsiloxane) (PDMS, Sylgard 184 Down Corning) stamps were obtained by replica molding of a prefabricated master made of parallel lines by mixing the curing agent 1:10 (v/v). The curing process was carried out for 3 h at 90 °C.

**2.3. Polarized Optical Microscopy (POM).** A commercial optical microscope (Nikon i-80) equipped with an epi-illuminator and crossed polarizers was used to inspect the crystal orientations and to follow the evolution of birefringence across the ferroelectric transition. The incident polarization direction was fixed, and the sample was rotated by using a rotation stage. Samples were mounted on a heating−cooling stage with optical access (Linkham TMHS600) connected to a TP94 controller, with a control of 0.1 °C. The resolution of POM using visible light is on the order of half the wavelength. To analyze the fine structure of FE domains, the higher spatial resolution technique that is used is piezoforce microscopy.

**2.4. Atomic Force Microscopy.** AFM images were recorded with a commercial AFM (MultiMode 8, Bruker) operating in tapping or peak-force mode under ambient conditions. Image analysis was done using open source SPM software Gwyddion (www.gwyddion.net).

**2.5. X-ray Diffraction.** Specular X-ray diffraction (XRD) measurements were carried out with a SmartLab Rigaku diffractometer equipped with a rotating copper anode ($\lambda_{Cu}$ = 1.54184 Å) followed by a parabolic mirror to collimate the incident parallel beam and a series of variable slits placed before and after the sample to control the beam size and detector acceptance, respectively. The beam resolution was 0.01°.

2D-GIXRD diffraction patterns were collected using the 2D Pilatus detector at the XRD1 beamline of the ELETTRA synchrotron facility in Trieste, Italy. The X-ray beam was characterized by an energy of 12.5 keV (corresponding to $\lambda$ = 1 Å) and a beam size of 200 × 200 $\mu m^2$. The grazing incident angle was fixed at $\alpha_i$ = 0.1° to maximize the diffraction signal coming from the nanostructured film at the top of the substrate.

**2.6. Raman spectroscopy.** Raman spectra were collected using a Renishaw microRaman equipped with a 632.8 nm He−Ne laser line. Raman scattering measurements were recorded in backscattering configuration using a long-working-distance 50× microscope objective. The laser spot was focused on the patterned structures. The samples were mounted in the heating−cooling stage, allowing the ferroelectric−paraelectric transition to be crossed .

**2.7. Piezoforce Microscopy.** The piezoforce microscopy (PFM) setup is made of a commercial probe head (NT-MDT, SMENA) with electronics and control software developed in-house.[17] PFM is an AFM working in contact mode where a conductive tip is employed in order to apply an ac voltage and detect the ferroelectric response.[18] In our setup, the ac voltage was applied via a function generator (Agilent 33220A), and a digital lock-in amplifier (Zurich, HF2LI) was employed to collect the data. The detection of vertical (VPFM) and torsional (LPFM) components of the cantilever response allows two vector components, in plane (the tip moves from left to right along the $x$ axis) and out of plane (cantilever deflection along the $z$ axis), to be simultaneously measured. The tip employed was made of doped Si with a cantilever spring constant of around 0.2 N/m (PPP-CONTROL-SPL). A dc voltage (10−30 V) was applied to the tip in order to switch the domains.

## 3. RESULTS AND DISCUSSION

DIPAB crystals present two well-known polymorphs: the first one is ferroelectrically active, has space group $P2_1$ (1-F), and presents needle shaped crystals; the second is not ferroelectrically active, its structure belongs to $P2_12_12_1$ (1-P form), and it presents block-shaped crystals eventually converted to 1-F after thermal annealing at 410 K.[10] In polymorph, the structure of crystals is generally driven by changing the evaporation environment (e.g., Gao et al.[12]), whereas in films, the crystalline structure of the deposit can be forced by interaction with substrates or by confinement. We profit from these two latter options by patterning DIPAB with the LCW technique to drive the molecule organization[14,15] in order to avoid the formation of polymorphs. Moreover, the LCW technique allows us to force the geometry of DIPAB deposits by defining a priori the size and the conformation of the stamp. With this aim, we printed micrometric stripes of DIPAB that were 1 $\mu$m wide (and thus optically accessible) on naturally oxidized Si


DOI: 10.1021/acs.langmuir.7b02102
Langmuir 2017, 33, 12859−12864

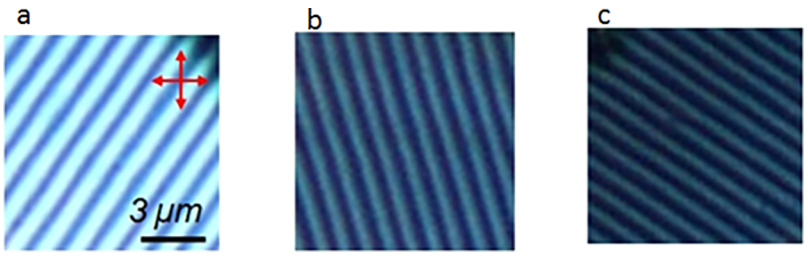


**Figure 2.** Reflection-mode polarized optical micrographs showing the contrast as a function of sample rotation relative to the polarizer−analyzer (P−A) pair. At a 0° relative angle (a), the contrast is maximized, whereas extinction is obtained at $\theta_e$ = 90°(c). (b) Intermediate condition at 45°. The exposure time is the same for (a) and (b), whereas image (c) is obtained with a 10× exposure time.

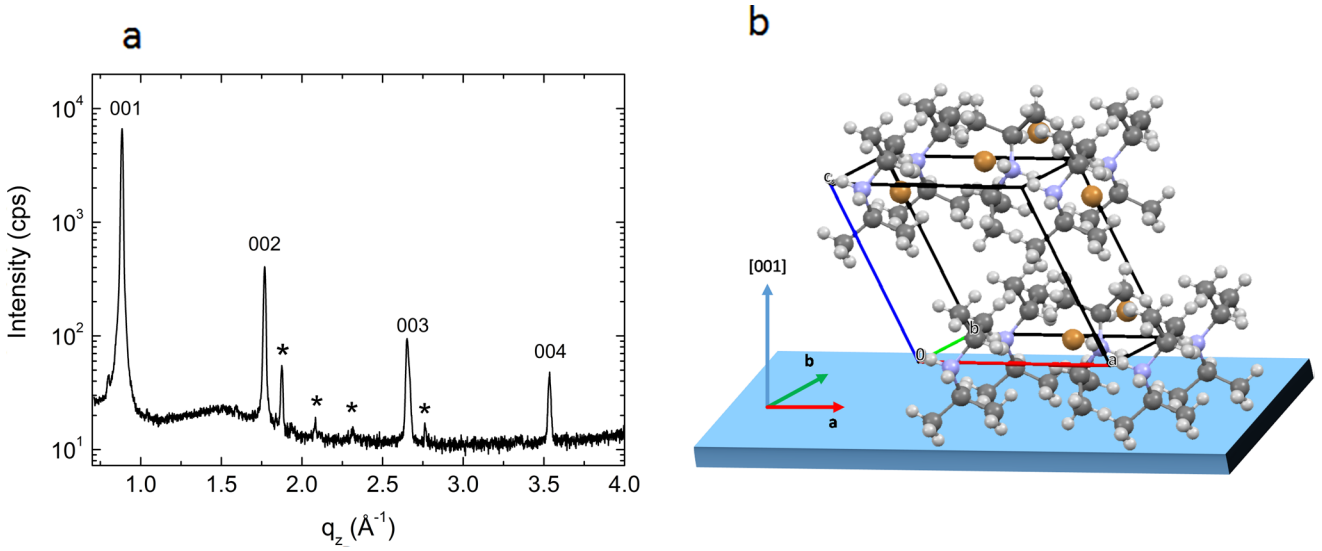


**Figure 3.** (a) Specular XRD scan performed on DIPAB crystals grown by LCW on $SiO_2$. Stars label peaks coming from reflections different from {00l}. (b) Schematic representation of the crystalline structure on the surface.

substrates (Si/$SiO_x$) by depositing 20 μL of 0.25 g/L and 0.15 g/L of DIPAB solutions in water.

AFM images of the printed structures reveal the formation of stripelike structures of 1 μm width (Figure 1b) according to the size of the stamp and thickness depending on the concentration of the solution. Using a 0.25 g/L solution, we obtained continuous stripes, and by using a more dilute solution, we occasionally observed discontinuous structures with variable thickness ranging from 10 to 150 nm (Figure 1c).

DIPAB microstripes show the typical behavior of optically anisotropic materials;[19] by POM, stripes appear to be gray, and their lightness depends on the crystal thickness (Figure 2). More than 95% of the stripes appear to be homogeneously colored, indicating that their thickness is homogeneous (as confirmed by AFM) over the entire stripes. Rotating the crystals vs the polarized light, stripes are extinguished in four positions at intervals of 90°. The evidence of light extinction of the complete stripes at defined orientation indicates that crystal coherence extends over the entire stripe. Because confinement in microchannels occurs under quasi-equilibrium conditions, the crystal nucleation centers are minimized, favoring the formation of larger crystal domains with respect to typical crystal dimension obtained with conventional thin film growth methods.[15]

To identify the crystalline structure of DIPAB-patterned films, XRD patterns were collected at room temperature. The specular scan, reported in Figure 3a, shows only the Bragg peaks characteristic of the ferroelectric monoclinic $P2_1$ phase ($a$ = 7.855, $b$ = 8.095, $c$ = 7.896, $\beta$ = 116.23°) indicating that the confinement by stamps prevents the formation of the nonferroelectric polymorph. The presence of the strong (00$l$) reflections point out that the stripes consist of crystallites preferentially oriented with the ($ab$) plane parallel to the substrate surface, although a small number of crystallites with different orientations is identified by the less-intense peaks (marked by stars in Figure 3). The polar axis for DIPAB is along the crystallographic $b$ axis;[9] therefore, the polarization is expected to be in plane.

More quantitative information was obtained by analyzing 2D-GIWAXS images collected using the X-ray beam perpendicular (Figure 4a) and parallel (Figure 4b) to the stripes. Figure 4c shows the 2D image simulated by the SimDiffraction code[20] with [001] texturing. The absence of the reflections coming from the (11$l$) planes in both experimental images indicates that crystallites also have a preferential orientation in the substrate plane, with the $a$ or $b$ axis lying parallel to the stripe direction as depicted in Figure 3b. The anisotropic spatial confinement due to the geometry of the channel (i.e., a few tens of nanometers in the vertical dimension, 1 μm in the width, and no confinement present along the channel) leads to a preferred orientation of anisotropic crystallites, with the growth axis ($b$ axis[12]) along the channel direction.

In addition to crystallization pathways, confinement is used to influence, screen, or control the formation of polymorphic



DOI: 10.1021/acs.langmuir.7b02102
Langmuir 2017, 33, 12859−12864

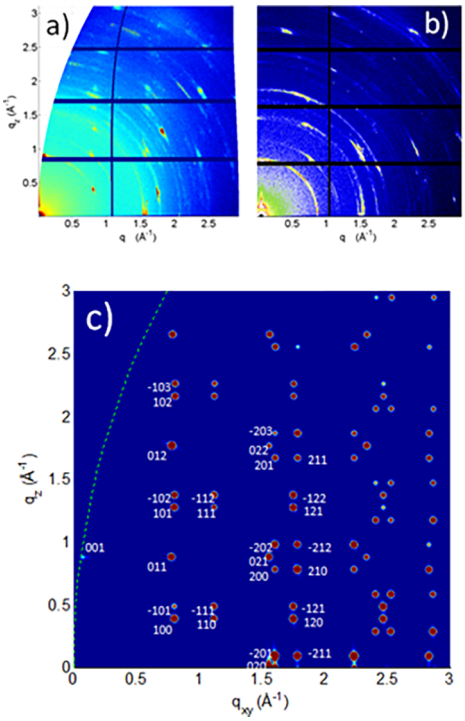


**Figure 4.** 2D-GIWAXS images collected for a patterned sample using the incident beam perpendicular (a) and parallel (b) to the stripe direction. (c) Simulation of the reciprocal space for a 1F phase with [001] texturing.

species.[21] In our specific case, it promotes the formation of the ferroelectric monoclinic $P2_1$ phase.

The mechanism and dynamics of the FE phase transitions have been characterized by Raman measurements as a function of temperature, ranging from 300 to 440 K. Figure 5a shows the temperature evolution of Raman spectra. Internal vibrations of diisopropylammonium cations manifest themselves in a complex Raman spectra having 63 normal vibrational modes.[22] Raman peaks above 2800 cm$^{-1}$ come from the vibrations of $-CH_3$ and $-NH_2$ groups. To analyze the transition of DIPAB in more detail, two Raman peaks were selected whose positions at 300 K are 803.2 and 835.6 cm$^{-1}$, and they are associated with symmetric and antisymmetric stretching vibrations of the C−N−C bond in the diisopropylammonium cations.[22] The Raman peak position shifts to lower frequency by increasing the temperature, and we can clearly identify the ferroelectric transition close to the nominal FE transition 425 K (Figure 5b). Above this temperature, the Raman spectra became extremely noisy, indicating an overall degradation of the compound.

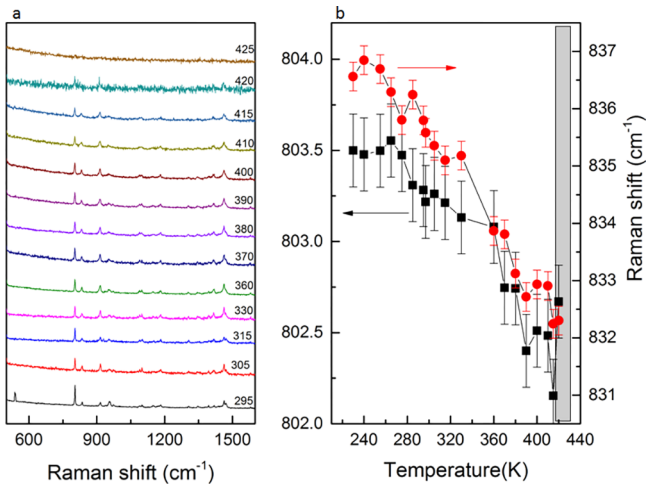


**Figure 5.** (a) Raman spectrum of DIPAB stripes at different temperatures. (b) Temperature dependence of the Raman peak position of the C−N−C bond in the diisopropylammonium cation. The gray rectangle indicates the transition region.

POM provides a visualization of the domain structure and allows the observation of domain evolution as a function of temperature (Figure 6). Optical images indicate that, until the temperature is far from the Curie temperature,[23] cross-polarized images present uniform regions within the stripes, indicating a large spatial coherence. Approaching $T_C$, we observe the formation of a multidomain structure with opposite contrast within stripes that can be interpreted as the nucleation and growth of inverted domains with slight misorientations of the crystal along the polarization axis.[8] Above $T_c$, the stripe structure is completely lost.

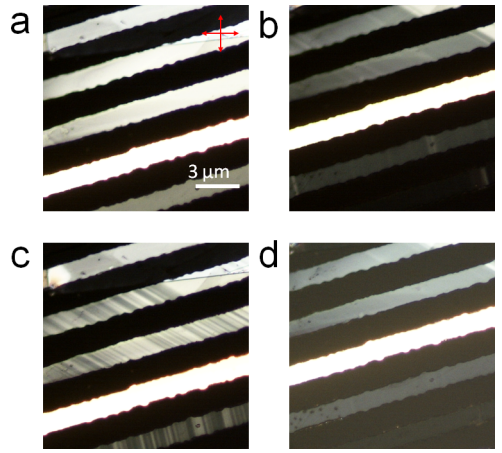


**Figure 6.** POM images collected across the Curie temperature at (a) 400, (b) 420, (c) 425, and (d) 430 K. The image at 425 K clearly shows the formation of antiparallel domains.

A detailed investigation of the coherence of ferroelectric domains has been carried out at RT with PFM (Figure 7) by comparing topographic images and corresponding vertical and longitudinal piezoresponse images on patterned films. On pristine samples, PFM images illustrate responses (Figure 7b,c) that depend on the thickness and dimensions of the DIPAB stripes, with a characteristic enhancement in the correspondence of the lateral edges. Such a perimeter effect is related to the morphology of the samples and is associated with the inhomogeneous potential distribution at the edge.[24] On a continuous microstripe (150 thick), a clear striped pattern is evident in VPFM images (indicated with an arrow in Figure 7b), whereas LPFM shows uniform images (Figure 7c). Such a contrast in VPFM corresponds to an antiparallel stripe domain configuration and is consistent with the ferroelectric configuration of DIPAB microcrystals obtained by wet techniques.[12,25] The incomplete DIPAB pattern obtained from a low-concentration solution (≤0.15 g/L) develops a domain structure with alternating contrast perpendicular to the stripe long axis in both VPFM and LPFM. By combining the domain structure with XRD results, we then expect that for complete


DOI: 10.1021/acs.langmuir.7b02102
Langmuir 2017, 33, 12859−12864

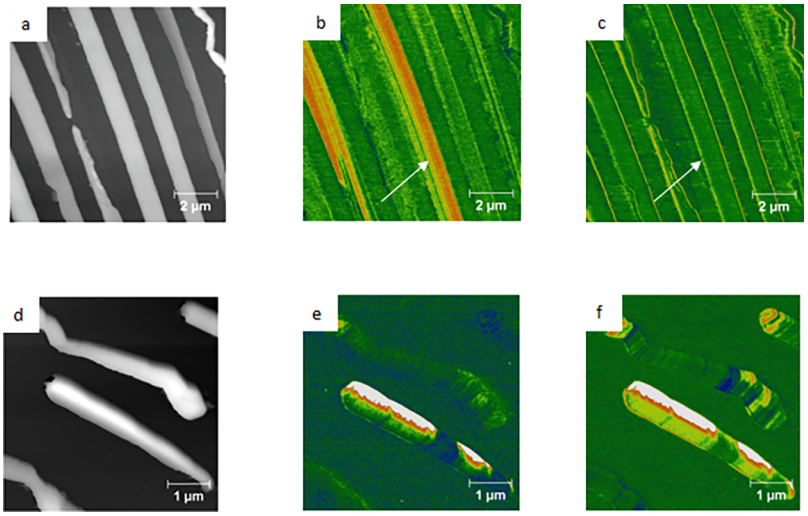


**Figure 7.** Typical topography (a, d), vertical PFM (b, e), and lateral PFM (c, f) of patterned structures ($z$ scale = 0−200 nm). For complete 150-nm-thick stripes, the PFM amplitude shows stripe domains only in the VPFM image (arrow in Figure 8b,c), whereas incomplete ones in the present domain have periodicity along the domain width in both VPFM and LPFM.

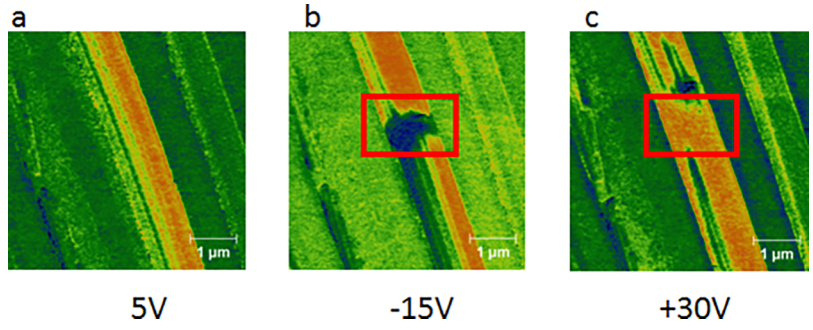


**Figure 8.** Electrical modification of the domain structure in a DIPAB deposit. (a) As-grown domain structure. (b) Electrically written domain structure formed by scanning with the PFM tip under −15 V dc. (c) Domain structure further modified by scanning with the PFM at a +30 V dc bias.

150-nm-thick stripes the polar $b$ axis is along the stripe axis whereas for incomplete ones the PFM signal is interpreted by assuming a nonperfect alignment of the polarization vector in the plane as a result of the application of an electric field along the $c$ axis. An additional investigation must be carried out in order to understand how the dimensionality impacts the formation of the energy of domains as well as the polarization orientation.

To explore the polarization dynamic, the switchability was checked on continuous stripes presenting striped domains. External electric fields were applied through the PFM tip by the application of a sequence of positive and negative voltage over the same area as evidenced in Figure 8. Notably, the switchability of ferroelectrics is directly utilized in ferroelectric data storage, where ferroelectric nanodomains serve as physical storage elements.[23] Typical resulting patterns are presented in Figure 8. A quite homogeneous opposite amplitude variation is obtained in the poled regions. The polarization can be switched only when the applied voltage is above 15 V. The domain modification extends over a distance larger than the point of voltage application: in Figure 8b,c, it is clearly visible that switchable domains develop along the polar axis (along the stripe) probably as a result of the inhomogeneous distribution of the tip-generated field.[26] The PFM signal is stable for several hours, excluding the contribution from electrostatic effects

## 4. CONCLUSIONS

Ferroelectric DIPAB-patterned structures have been obtained on Si/$SiO_x$ by a solution-based LCW technique. Confinement drives the DIPAB crystalline phase and crystal orientations, achieving highly coherent ferroelectric microstructures with the polarization axis pointing into the plane. Exploiting the strong tendency of DIPAB to crystallize, we can control the morphology of patterned films from continuous stripes to isolated microcrystals simply acting on solution concentrations and stamp geometries. The ferroelectric domain pattern was found to vary depending on the deposit dimensions, suggesting additional surface-energy-related mechanisms in defining the polarization vector orientations.

Remarkably, we succeeded in obtaining submillimeter-long stripes with uniform thickness and polarization standing along the stripe axis. In such crystals, polarization is switched by the sequential application of positive and negative voltage, demonstrating the possibility of address memory devices. Results indicate that LCW is an attractive technique for thin film deposition of MF with superior properties with respect to the solution-based method, surpassing the current restriction of processability of ferroelectric molecular compounds.



DOI: 10.1021/acs.langmuir.7b02102
*Langmuir* 2017, 33, 12859−12864

## AUTHOR INFORMATION


### Corresponding Author

*Phone:+39 0516398509. Fax:+39 0516398540. E-mail: ilaria.bergenti@cnr.it.

### ORCID

Ilaria Bergenti: 0000-0003-0628-9047

Giampiero Ruani: 0000-0001-9326-0490


### Notes

The authors declare no competing financial interest.

## ACKNOWLEDGMENTS

E.W. acknowledges the Swedish Research Council and the Swedish Research Council Formas for financial support.

## REFERENCES


(1) Auciello, O.; Scott, J. F.; Ramesh, R. The physics of ferroelectric memories. *Phys. Today* **1998**, *51* (7), 22−27.

(2) Dawber, M.; Rabe, K. M.; Scott, J. F. Physics of thin-film ferroelectric oxides. *Rev. Mod. Phys.* **2005**, *77* (4), 1083−1130.

(3) You, Y.-M.; Liao, W.-Q.; Zhao, D.; Ye, H.-Y.; Zhang, Y.; Zhou, Q.; Niu, X.; Wang, J.; Li, P.-F.; Fu, D.-W.; Wang, Z.; Gao, S.; Yang, K.; Liu, J.-M.; Li, J.; Yan, Y.; Xiong, R.-G. An organic-inorganic perovskite ferroelectric with large piezoelectric response. *Science* **2017**, *357* (6348), 306−309.

(4) Furukawa, T. Structure and functional properties of ferroelectric polymers. *Adv. Colloid Interface Sci.* **1997**, *71*−*72*, 183−208.

(5) Ryu, J.; No, K.; Kim, Y.; Park, E.; Hong, S. Synthesis and Application of Ferroelectric Poly(Vinylidene Fluoride-co-Trifluoroethylene) Films using Electrophoretic Deposition. *Sci. Rep.* **2016**, *6*, 36176.

(6) Horiuchi, S.; Tokunaga, Y.; Giovannetti, G.; Picozzi, S.; Itoh, H.; Shimano, R.; Kumai, R.; Tokura, Y. Above-room-temperature ferroelectricity in a single-component molecular crystal. *Nature* **2010**, *463* (7282), 789−792.

(7) Horiuchi, S.; Tokura, Y. Organic ferroelectrics. *Nat. Mater.* **2008**, *7* (5), 357−366.

(8) Shi, P.-P.; Tang, Y.-Y.; Li, P.-F.; Liao, W.-Q.; Wang, Z.-X.; Ye, Q.; Xiong, R.-G. Symmetry breaking in molecular ferroelectrics. *Chem. Soc. Rev.* **2016**, *45* (14), 3811−3827.

(9) Fu, D.-W.; Cai, H.-L.; Liu, Y.; Ye, Q.; Zhang, W.; Zhang, Y.; Chen, X.-Y.; Giovannetti, G.; Capone, M.; Li, J.; Xiong, R.-G. Diisopropylammonium Bromide Is a High-Temperature Molecular Ferroelectric Crystal. *Science* **2013**, *339* (6118), 425−428.

(10) Jiang, C.; Lin, H.; Luo, C.; Zhang, Y.; Yang, J.; Peng, H.; Duan, C.-G. Crystal growth and dynamic ferroelectric hysteresis scaling behavior of molecular ferroelectric diisopropylammonium bromide. *J. Cryst. Growth* **2016**, *438*, 25−30.

(11) Fu, D.-W.; Zhang, W.; Cai, H.-L.; Ge, J.-Z.; Zhang, Y.; Xiong, R.-G. Diisopropylammonium Chloride: A Ferroelectric Organic Salt with a High Phase Transition Temperature and Practical Utilization Level of Spontaneous Polarization. *Adv. Mater.* **2011**, *23* (47), 5658−5662.

(12) Gao, K.; Xu, C.; Cui, Z.; Liu, C.; Gao, L.; Li, C.; Wu, D.; Cai, H.-L.; Wu, X. S. The growth mechanism and ferroelectric domains of diisopropylammonium bromide films synthesized via 12-crown-4 addition at room temperature. *Phys. Chem. Chem. Phys.* **2016**, *18* (11), 7626−7631.

(13) Poddar, S.; Lu, H.; Song, J.; Goit, O.; Valloppilly, S.; Gruverman, A.; Ducharme, S. Fabrication of diisopropylammonium bromide aligned microcrystals with in-plane uniaxial polarization. *J. Phys. D: Appl. Phys.* **2016**, *49* (50), 505305.

(14) Cavallini, M.; Gentili, D.; Greco, P.; Valle, F.; Biscarini, F. Micro- and nanopatterning by lithographically controlled wetting. *Nat. Protoc.* **2012**, *7* (9), 1668−1676.

(15) Gentili, D.; Valle, F.; Albonetti, C.; Liscio, F.; Cavallini, M. Self-Organization of Functional Materials in Confinement. *Acc. Chem. Res.* **2014**, *47* (8), 2692−2699.

(16) Xia, W.; Peter, C.; Weng, J.; Zhang, J.; Kliem, H.; Jiang, Y.; Zhu, G. Epitaxy of Ferroelectric P(VDF-TrFE) Films via Removable PTFE Templates and Its Application in Semiconducting/Ferroelectric Blend Resistive Memory. *ACS Appl. Mater. Interfaces* **2017**, *9* (13), 12130−12137.

(17) Cheng, C.-E.; Liu, H.-J.; Dinelli, F.; Chen, Y.-C.; Chang, C.-S.; Chien, F. S.-S.; Chu, Y.-H. Revealing the flexoelectricity in the mixed-phase regions of epitaxial BiFeO3 thin films. *Sci. Rep.* **2015**, *5*, 8091.

(18) Gruverman, A.; Auciello, O.; Tokumoto, H. Imaging and control of domain structures in ferroelectric thin films via scanning force microscopy. *Annu. Rev. Mater. Sci.* **1998**, *28*, 101−123.

(19) Melucci, M.; Favaretto, L.; Zanelli, A.; Cavallini, M.; Bongini, A.; Maccagnani, P.; Ostoja, P.; Derue, G.; Lazzaroni, R.; Barbarella, G. Thiophene−Benzothiadiazole Co-Oligomers: Synthesis, Optoelectronic Properties, Electrical Characterization, and Thin-Film Patterning. *Adv. Funct. Mater.* **2010**, *20* (3), 445−452.

(20) Breiby, D. W.; Bunk, O.; Andreasen, J. W.; Lemke, H. T.; Nielsen, M. M. Simulating X-ray diffraction of textured films. *J. Appl. Crystallogr.* **2008**, *41* (2), 262−271.

(21) Hamilton, B. D.; Ha, J.-M.; Hillmyer, M. A.; Ward, M. D. Manipulating Crystal Growth and Polymorphism by Confinement in Nanoscale Crystallization Chambers. *Acc. Chem. Res.* **2012**, *45* (3), 414−423.

(22) Gao, K.; Gu, M.; Qiu, X.; Ying, X. N.; Ye, H.-Y.; Zhang, Y.; Sun, J.; Meng, X.; Zhang, F. M.; Wu, D.; Cai, H.-L.; Wu, X. S. Above-room-temperature molecular ferroelectric and fast switchable dielectric of diisopropylammonium perchlorate. *J. Mater. Chem. C* **2014**, *2* (46), 9957−9963.

(23) Scott, J. F. Applications of Modern Ferroelectrics. *Science* **2007**, *315* (5814), 954−959.

(24) Peter, F.; Rüdiger, A.; Dittmann, R.; Waser, R.; Szot, K.; Reichenberg, B.; Prume, K. Analysis of shape effects on the piezoresponse in ferroelectric nanograins with and without adsorbates. *Appl. Phys. Lett.* **2005**, *87* (8), 082901.

(25) Lu, H.; Li, T.; Poddar, S.; Goit, O.; Lipatov, A.; Sinitskii, A.; Ducharme, S.; Gruverman, A. Statics and Dynamics of Ferroelectric Domains in Diisopropylammonium Bromide. *Adv. Mater.* **2015**, *27* (47), 7832−7838.

(26) Rodriguez, B. J.; Nemanich, R. J.; Kingon, A.; Gruverman, A.; Kalinin, S. V.; Terabe, K.; Liu, X. Y.; Kitamura, K. Domain growth kinetics in lithium niobate single crystals studied by piezoresponse force microscopy. *Appl. Phys. Lett.* **2005**, *86* (1), 012906.




DOI: 10.1021/acs.langmuir.7b02102
*Langmuir* 2017, 33, 12859−12864